Contents

List of Figures

List of Tables

CHAPTER 2

Investigating the Unification of LOFAR-detected Sources in the Boötes Field

"There are some oddities in the perspective with which we see the world. The fact that we live at the bottom of a deep gravity well, on the surface of a gas-covered planet going around a nuclear fireball 90 million miles away and think this to be normal is obviously some indication of how skewed our perspective tends to be."
−Douglas Adams−

Low radio frequency surveys are important for testing unified models of radio-loud quasars and radio galaxies. The steep-spectrum isotropic radio emission of these sources allows for orientation-free sample selection at low radio frequencies. Sources similar in size but differently oriented will show different projected linear sizes, and measuring these projected sizes gives the orientation of a source with respect to the line of sight. We use a new radio survey of the Boötes field at 150 MHz made with the Low Frequency Array (LOFAR) to select a sample of radio sources, and identify radio galaxies and quasars using cross-matched multi-wavelength information from the AGN and Galaxy Evolution Survey (AGES), which also provides spectroscopic redshifts. Within the LOFAR sample we find that radio sources with steep spectra have projected linear sizes that are on average 4.4 ± 1.4 times larger than those with flat spectra. We also find that the projected linear sizes of radio galaxies are on average 3.1 ± 1.0 times larger than those of quasars. We combine these results with two previous surveys and find that the linear size of sources is dependent on redshift but not on power. We also find that the linear size ratio of radio galaxies to quasars does not evolve with either redshift or power. The quasar fraction at low redshifts is ~ 0.2 and is positively correlated with the linear size ratio at higher redshifts. We conclude that the data are consistent with an orientation-based unification scheme.

Morabito, L. K., Williams, W. L., Saxena, A., Duncan, K., Röttgering, H. J. A., et al.
In preparation

2.1 Introduction

Active galactic nuclei (AGN) produce high nuclear luminosities that cannot be explained by star formation alone. They are believed to be powered by central super-massive black holes. AGN can exhibit a wide variety of observational characteristics, including high luminosities in the optical and near-IR, strong emission lines from ionised gas, and high mid-IR luminosities. AGN which have strong emission lines in their spectra are classified as Type 1 or Type 2 based on the emission line properties. Type 1 AGN show broad and narrow emission lines while Type 2 AGN show only narrow emission lines.

Under the current unification paradigm (Antonucci, 1993; Urry & Padovani, 1995) Type 1 and Type 2 AGN exhibit different observed characteristics due to the presence of a dusty structure or torus that will obscure the accretion disk and broad line region depending on viewing angle to the AGN. Those AGN which exhibit broad emission lines are associated with bright optical point sources, leading to the term 'quasi-stellar object' or quasar. Type 1 AGN are oriented such that the optical quasar and broad line emission regions are seen directly without obscuration from the torus. Type 2 AGN are oriented such that the broad line emission region and optical quasar are obscured by the dusty torus, and not directly visible.

About 10 per cent of AGN exhibit extended powerful radio emission in the form of jets that extend far beyond the host galaxy and can provide an indication of orientation. Low radio frequency surveys are important for selecting these objects in an orientation-independent way, as high-frequency surveys are biased towards core-dominant objects where the jets are pointed towards the observer.

Radio-loud AGN comprise two populations, believed to be powered by different accretion methods. Radio galaxies that exhibit strong emission lines in the optical regime are referred to as high-excitation radio galaxies (HERGs). HERGs can be either Type 1 or Type 2 AGN. The AGN in HERGs are thought to be powered via a geometrically thin and optically thick accretion disk (Shakura & Sunyaev, 1973). The accretion disk is believed to be fed by large central repositories of cold gas (e.g., Larson, 2010), which has led to the name 'cold-mode' accretion (Best et al., 2005).

The second type of radio-loud AGN lack the strong emission lines seen in HERGs, and are thus termed low-excitation radio galaxies (LERGs). They also lack evidence for a dusty torus in their infrared emission (e.g., Tasse et al., 2008; Ogle et al., 2006; Whysong & Antonucci, 2004), as well as evidence for a full accretion disk (e.g., Hardcastle et al., 2006; Evans et al., 2006). LERGs are thought to be powered by 'hot-mode' accretion processes, where hot gas is

accreted via advection-dominated accretion or radiatively inefficient accretion flows (e.g., Narayan & Yi, 1994; Quataert, 2001; Ho, 2008). For these reasons the non-radio spectral energy distributions of LERGs are not expected to show strong orientation effects. Best & Heckman (2012) showed that LERGs dominate the population of low-power ($P_{1.4\mathrm{GHz}} \lesssim 10^{25}\,\mathrm{W\,Hz^{-1}}$) sources at least in the local universe, and tend to be associated with edge-dimmed radio jets of Fanaroff-Riley Class I objects (FRI; Fanaroff & Riley, 1974).

The discovery of super-luminal motion in radio jets was strong evidence that some radio sources have their jets aligned close (within ~ 15 degrees) to the line of sight (Barthel et al., 1989). Radio sources with beamed flat-spectrum cores consistent with super-luminal motion should have smaller projected sizes on average than steep-spectrum radio sources with jets oriented further from the line of sight. For HERGs this scenario can be related to the difference between radio galaxies and quasars to the obscuring torus being viewed edge on in radio galaxies, hiding the optical quasar emission. Radio galaxies will therefore have radio jets preferentially oriented closer to the plane of the sky, while quasars will have radio jets closer to the line of sight.

Barthel (1989) used the 3CRR survey of radio sources at 178 MHz (Laing et al., 1983) to study the projected linear sizes for 42 radio sources with optical identifications for $0.5 \leq z \leq 1$. Barthel found that there was a division between radio sources: those associated with quasars were on average 2.2 times smaller than the other radio sources. The 3CRR sample is now 100 per cent spectroscopically complete, and classifications based on emission line ratios have been used to identify HERGs (which are expected to show orientation effects) and LERGs (which are not expected to show orientation effects). The high limiting flux density of the survey means that only 13 per cent have been found to be LERGs (Willott et al., 1999), and are therefore were not a large contaminant in studies previous to this classification.

Follow up studies have tended to confuse the issue. A reassessment of the 3CRR sample found systematically larger sizes of radio-loud AGN (hereafter radio galaxies) compared to radio-loud quasars only for redshifts above 0.5. For lower redshifts, radio galaxies were on average larger than radio-loud quasars but only when their cumulative linear sizes were above $\lesssim 400$ kpc Singal (2014). Singal & Singh (2013) also studied the linear sizes of a 98 per cent spectroscopically complete sample selected at 408 MHz (Best et al., 1999), finding that only at redshifts larger than 1 were the linear sizes of radio galaxies systematically larger than those of quasars. The authors made no attempt to remove LERGs from the sample, but argued that they would have to be a large part of the sam-

ple to change the results. However these studies still only cover a small part of the power−redshift ($P-z$) diagram, and it is important to collect more information to investigate this further.

In this study we use a new low frequency radio survey of the Boötes field (Williams et al., 2016) with the Low Frequency Array (LOFAR; van Haarlem et al., 2013) to investigate the unification of radio sources in two ways. First, we look at the difference in projected linear sizes of flat- and steep-spectrum sources, without any classification from other wavelengths. Second, we investigate the difference in projected linear sizes of cold-mode accretion sources by splitting our sample of HERGs into *quasars* and *radio galaxies* using available multi-wavelength data including spectroscopic redshifts and quasar classifications from the AGN and Galaxy Evolution Survey (AGES; Kochanek et al., 2012). It is difficult to measure properly the sizes of edge-dimmed FR I sources, and we make a power cut at $P_{150\mathrm{MHz}} > 10^{25.5}\,\mathrm{W\,Hz^{-1}}$ to exclude these sources as well as star-forming galaxies at lower powers (Saxena et al., in preparation). This means our sample is likely to be dominated by HERGs, although it is difficult to determine this based on broad-band photometry alone (Janssen et al., in preparation).

The new LOFAR catalogue contains over 6,000 radio sources to an rms depth of $\sim 120-150\,\mu\mathrm{Jy\ beam^{-1}}$ at 150 MHz. While previous samples used to test orientation-based unification probed high luminosity sources over large areas of the sky, the deep LOFAR data probes a large number of fainter sources over a smaller area. This adds a substantial number of sources to the P−z diagram at lower powers across all redshifts.

Section 2.2 first describes the LOFAR survey, the multi-wavelength data, and the selection of quasars and radio galaxies. Results from the LOFAR survey are presented in Section 2.3. The LOFAR results combined with two previous samples are presented in Section 2.4. Discussion and conclusions follow in Sections 2.5 and 2.6. Throughout the paper we assume a ΛCDM concordance cosmology with $H_0 = 67.8\ \mathrm{km\,s^{-1}\,Mpc^{-1}}$, $\Omega_\mathrm{m} = 0.308$, and $\Omega_\Lambda = 0.692$, consistent with Planck Collaboration et al. (2015). Spectral index is defined as α with flux density $S \propto \nu^\alpha$.

2.2 The Boötes Field Data

In this section, we first present the pre-existing multi-wavelength data, the new LOFAR Boötes survey, and then the cross-matching of the radio and multi-wavelength data and measurement of angular radio sizes.

2.2.1 AGES: Multi-wavelength Data

The NOAO Deep Wide-Field Survey (NDWFS; Jannuzi & Dey, 1999) covers 9 deg square of the Boötes field with deep optical to near-infrared data (B_W, R, I, J, K). Ancillary data at longer wavelengths covers the near to mid-infrared (IRAC 3.6, 4.5, 5.8, and 8.0μm, and MIPS 24μm). Kochanek et al. (2012) used the combination of all 10 bands and complementary ultraviolet, radio, and X-ray data to construct a well defined sample of galaxies and AGN for a targeted spectroscopic survey. This AGN and Galaxy Evolution Survey (AGES) covers 7.7 deg square of the Boötes field and provides spectroscopic redshifts for 18,163 galaxies (to I =20 mag) and 4,764 AGN candidates (to I =22.5 mag) measured with the Hectospec instrument on the MMT. The NDWFS contains more than 2 million optical sources, and Kochanek et al. (2012) aimed to provide a complete sample of AGN and a statistically robust (via random sparse sampling) sample of normal galaxies. For this paper we are interested only in the AGN sample.

All AGN candidates in Kochanek et al. (2012, hereafter K12) were targeted for spectroscopic observations. From 8977 AGN candidates, spectra were taken for 7102 and redshifts obtained for 4764 (after excluding Galactic stars, which made up 9 per cent of successful redshifts). Spectroscopic information is therefore available for $\sim$ 53 per cent of AGN in AGES. For the sources with spectroscopic information, K12 also provide five different AGN classifications that rely on different bands of the multi-wavelength data (described in detail in K12). AGN can be selected based on compact, bright optical morphology, complex near-IR selections (based on Stern et al., 2005), bright mid-IR luminosities, the presence of X-ray point sources, and radio detections at 1.4 GHz.

To divide the LOFAR-detected sources into quasars and radio galaxies, we identify quasars as those objects satisfying the optical and/or mid-IR colour criteria (in line with above), and the rest of our sample is therefore defined as radio galaxies. We check that all of the radio galaxies satisfy the mid-IR 24 μm criteria (as above), which indicates the presence of a dusty torus (and these sources are therefore not likely to be LERGs).

2.2.2 AGES/LOFAR sample completeness

We wish to determine if the results of this study will be biased by only using sources with spectroscopic information. To do this we examine the radio angular size and redshift distributions for the 1433 sources which have $I \leq 22.5$. We compare the distributions for sources with spectroscopic redshifts (from AGES) and sources which have photometric redshifts (from Duncan et al., in preparation). These are shown in Fig. 2.1. Overall, the histograms have similar distribu-

tions, except for an excess in the photometric redshift distribution for $1.4 \lesssim z \lesssim 2$ ($0.15 \lesssim \log(1+z) \lesssim 0.3$. Examining the distributions of spectroscopic redshifts for radio galaxies and qausars shows that the two populations have similar distributions. The discrepancy between spectroscopic and photometric redshifts must therefore come from the other cross-matched galaxies in the sample, which are generally at lower powers and excluded from our analysis. This indicates that our results will not be biased towards certain spectral types by limiting the sample to only sources with spectroscopic redshifts.

We find that the distributions of the radio angular size, which is the parameter we are interested in for this study, are quite similar (see right panel of Fig. 2.1). We thus conclude that we are not missing populations of systematically smaller or larger objects, and do not expect our results to change if the sample were expanded.

2.2.3 LOFAR Boötes Survey

The catalogue from Williams et al. (2016) contains a total of 6,275 radio sources within 19 deg^2. The rms varies over the field of view, and sources with peak fluxes exceeding a threshold of 5σ above the local rms were included in the final catalogue. The rms is less than $120\,\mu$Jy beam^{-1} at the centre and more than 50 per cent of the field of view has rms noise less than $180\,\mu$Jy beam^{-1}. The average rms noise at the edges of the optical coverage is approximately $150\,\mu$Jy beam^{-1}. The resolution of the LOFAR image is 5.6×7.4 arcsec, with average positional accuracy of ~0.4 arcsec.

The sources in the catalogue are divided into classes based on radio morphology. Here we consider only single sources or extended sources with a radio core (VClass 1/11) and double sources with no obvious radio core (VClass 2/21). These will be mostly FR II, FR I, or unresolved sources. We make a power cut at $10^{25.5}\,\mathrm{W\,Hz^{-1}}$ to exclude lower power sources which are either star forming galaxies or more likely to have FR I morphology. Since FR I sources are dimmer at the edges, their linear sizes are not well defined. The other morphological classifications only make up 0.1 per cent of the catalogue, and are either diffuse or complex, and not expected to be the radio sources in which we are interested.

Radio Luminosity Functions

We compare the radio luminosity functions (RLFs) for our sample with model RLFs from Rigby et al. (2011). The observed RLF for the LOFAR sample with $P_{150} \geq 10^{25.5}\,\mathrm{W\,Hz^{-1}}$ has similar behaviour to the model RLF, i.e. the trends in space density are the same, suggesting that the sample is representative of the

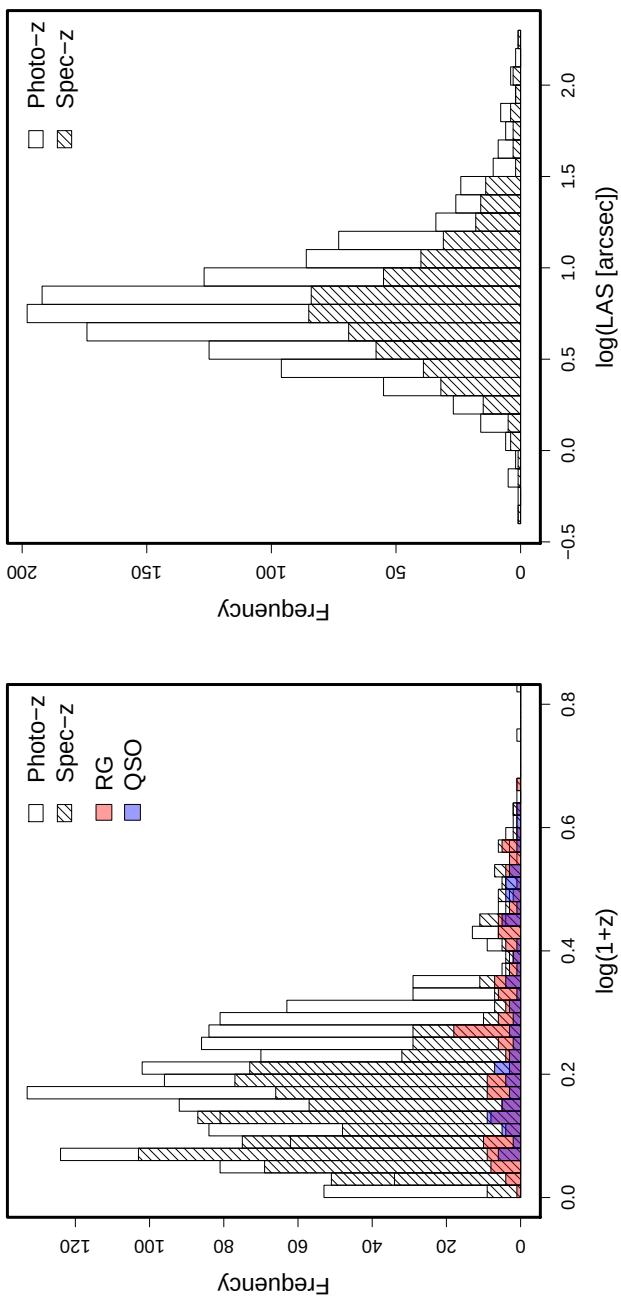

Figure 2.1: Comparison of redshift and radio angular size distributions for AGN from AGES which have $I \leq 22.5$ and LOFAR-detected radio emission. *Left:* Distribution of redshifts for sources with photometric redshifts (unfilled histogram) and spectroscopic redshifts (hatched histogram). *Right:* Distribution of radio largest angular size (LAS) for sources with photometric redshifts (unfilled histogram) and spectroscopic redshifts (hatched histogram).

entire population. Introducing higher power cuts in the LOFAR sample changes the RLF, and the space density of radio sources in the LOFAR sample drops off sharply above $z = 2$. We therefore do not consider higher power cuts in this analysis.

Cross-Matching and Measuring Sizes

Within the AGES footprint there are 3584 LOFAR detected sources. From a catalogue built from NDWFS multi-wavelength data (Brown et al., 2007, 2008), Williams (2015) identified 3106 galaxies to be associated with the radio sources. We cross-matched the optical positions of these galaxies with sources in the AGES catalogue within $1''$using TOPCAT (Taylor, 2005) and found 1106 sources with spectroscopic redshifts.

There are 60 sources with spectroscopic redshifts and $P_{150} \geq 10^{25.5}\,\mathrm{W\,Hz^{-1}}$. The angular sizes of these 60 sources were measured as the diameter of the smallest circle enclosing the source at a level of 5σ above the local rms. The centre of the circle may not correspond to the optical source. The size bent sources may be underestimated since we do not measure along the jets. As this fraction is small, this will have a negligible impact on the overall trends.

2.3 LOFAR Results

In this section we present the results for the LOFAR sample. First we investigate the linear sizes of flat and steep-spectrum radio sources, without any further knowledge of the type of host galaxy. We then investigate whether the linear sizes of quasars and radio galaxies, as identified from the multi-wavelength data, are different. This equates to a test of unification through orientation of HERGs, which are powered by cold-mode accretion. In all cases we use only the 60 sources with $P_{150} \geq 10^{25.5}\,\mathrm{W\,Hz^{-1}}$.

2.3.1 Flat vs. steep-spectrum Sources

First we test whether there is a systematic difference in projected linear sizes of flat- and steep-spectrum sources. Using the complementary 1.4 GHz data from a deep Westerbork survey of the Boötes field (de Vries et al., 2002), we calculated the spectral index between 150 MHz and 1.4 GHz and found 11 flat-spectrum objects with $\alpha > -0.5$ (18 per cent). Fig. 2.2 shows the cumulative linear sizes of the flat and steep-spectrum objects and the distribution of sources in the $P - z$ plane. The average redshifts of the two types of sources are $\bar{z} = 1.23$ for the steep-spectrum sources and $\bar{z} = 1.81$ for the flat-spectrum sources. The

difference in angular distance D_A at these two redshifts could make one group of sources appear systematically larger or smaller, so we use the ratio of $D_A(z = 1.81)/D_A(z = 1.23) = 1.01$ to correct the sizes of the steep-spectrum sources so they are comparable to those of the flat-spectrum sources. The projected linear sizes of steep-spectrum sources are on average 4.4±1.4 times larger than those of the flat-spectrum sources.

2.3.2 Quasars vs. Radio Galaxies

Next we test whether there is a systematic difference in the projected linear sizes of radio galaxies and quasars. We identify the quasars and radio galaxies using the AGES criteria as described in Section 2.2.1. The final sample has 44 radio galaxies and 16 quasars above a power cut of $10^{25.5}\,\mathrm{W\,Hz^{-1}}$, with average redshifts of $z = 1.16$ and $z = 1.84$. The cumulative linear sizes and distribution in the $P - z$ plane are shown in Fig. 2.3. The linear sizes of the radio galaxies are corrected for the ratio of $D_A(z = 1.84)/D_A(z = 1.16)$ so the sizes of one sample will not appear systematically larger or smaller. The radio galaxies have projected linear sizes that are 3.1±1.0 times larger than those of quasars.

2.4 Comparison with Previous Samples

In this section we first describe two previous samples that have been used to test the unification of radio galaxies and quasars. We then take these two samples and the new LOFAR sample and divide each into two redshift bins to study the properties of the projected linear sizes of radio galaxies and quasars using all available data.

2.4.1 3CRR Sample

Barthel (1989) used the 3CRR catalogue (Laing et al., 1983) to show the smaller cumulative linear sizes of quasars when compared to radio galaxies within the redshift range $0.5 < z < 1$. Since then, much more detailed optical information has become available. The 3CRR sample is now 100 per cent spectroscopically complete. In addition, near infrared spectroscopy allowed for the identification of HERGs and LERGs, using the equivalent width of [O III] and the ratio of [O II]/[O III] (Willott et al., 1999; Grimes et al., 2004). We use the sample from Willott et al. (1999)[1], which has HERG and LERG classifications as well as spectroscopic redshifts and largest angular sizes. We remove LERGs from the sample. The final number of sources is 170, of which 111 are radio galaxies and

[1] Available at http://astroherzberg.org/people/chris-willott/research/3crr/

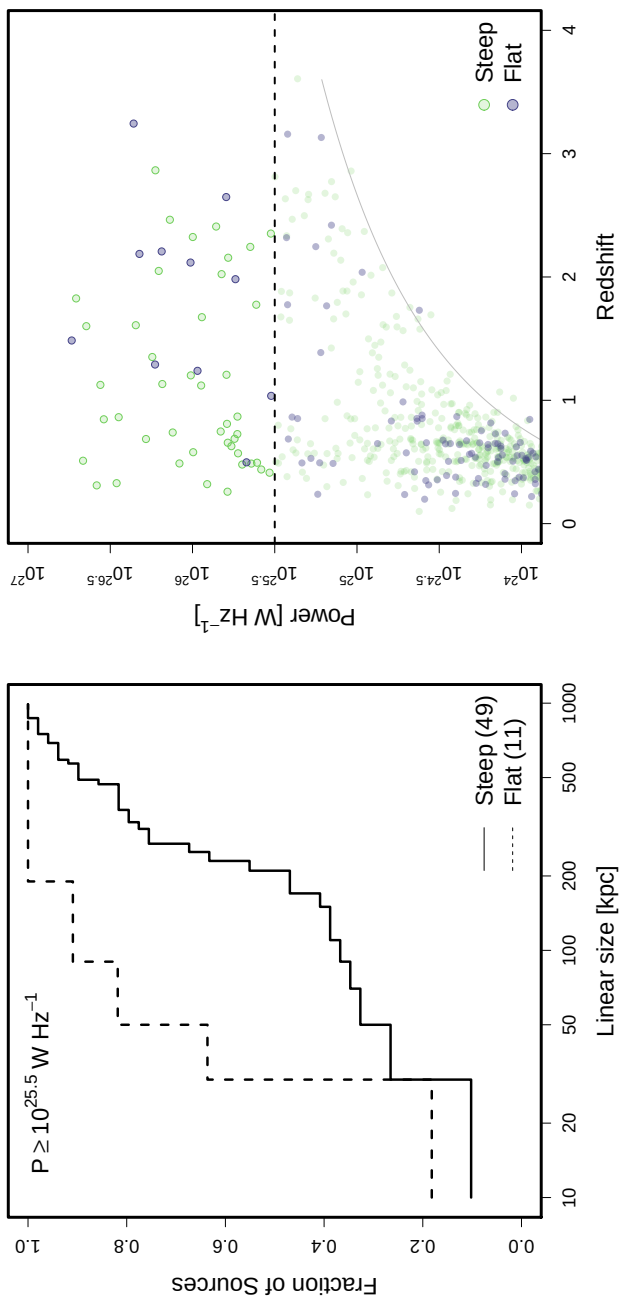

Figure 2.2: *Left:* Cumulative linear sizes for flat-spectrum and steep-spectrum radio sources are shown by the solid and dashed lines, respectively. The number of sources in each sample is indicated in parentheses in the legends. *Right:* The $P - z$ diagram. The horizontal dashed line indicates the power cut of $10^{25.5}\,\mathrm{W\,Hz^{-1}}$. The light gray line shows the flux limit for the survey.

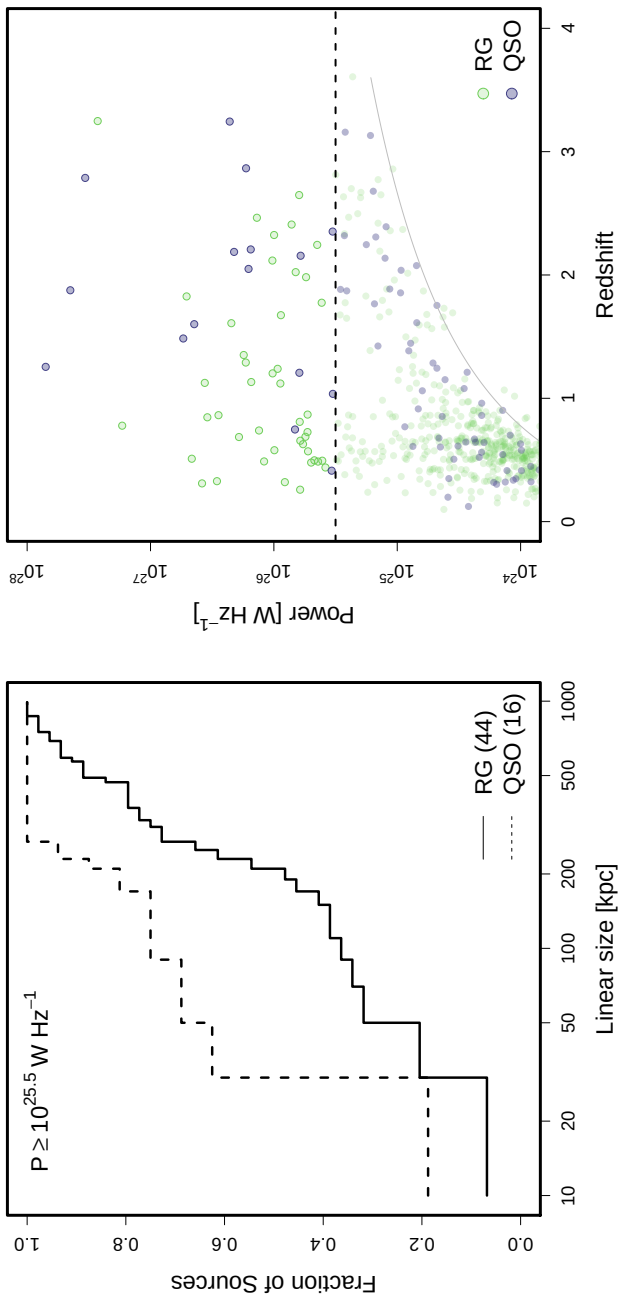

Figure 2.3: *Left:* Cumulative linear sizes for radio galaxies (RG) and quasars (QSO) are shown by the solid and dashed lines, respectively. The number of sources in each sample is indicated in parentheses in the legends. *Right:* The $P-z$ diagram. The horizontal dashed line indicates the power cut of $10^{25.5}\,\mathrm{W\,Hz^{-1}}$. The light gray line shows the flux limit for the survey.

59 are quasars. The mean redshifts are $z = 0.49$ for radio galaxies and $z = 0.82$ for quasars.

2.4.2 Molonglo Radio Catalogue Sample

We use Molonglo Radio Catalogue (MRC) 1 Jy Radio Source Survey (Kapahi et al., 1998a), and a complete quasar subset (Kapahi et al., 1998b; Baker et al., 1999). For this sample there are 349 object which have spectroscopic redshifts and measured angular sizes. This sample does not provide HERG/LERG identification, and the inclusion of LERGs may add radio sources with random orientation (i.e., not preferentially in the sky) to the sample. Since LERGs either lack or have a truncated accretion disk, they are less likely to be classified as quasars and therefore will slightly decreasing the average sizes of radio galaxies. There are 264 radio galaxies and 88 quasars. The radio galaxies have a mean redshift of $z = 0.75$ and the quasars have a mean redshift of $z = 1.13$. The average size of radio galaxies for the complete MRC sample is only 145 kpc, which is notably lower than the average radio size of sources in the LOFAR or 3CRR sample, and even smaller than the average size of quasars in the entire MRC sample.

2.4.3 Results

Each sample covers a different portion of the $P - z$ plane and we treat them separately, dividing each sample into low and high redshift bins. We determined the dividing redshift for each sample such that about half of the sample lies in each redshift bin, but without letting the number of quasars drop below 5 in a bin. The dividing redshifts used were: $z = 1.5$ (LOFAR), $z = 1$ (MRC), and $z = 0.5$ (3CRR). In each bin, we count the number of radio galaxies and quasars, and measure the mean values of power, redshift, and linear sizes for each type of source. These are listed in Tab. 2.1. We use the linear sizes to calculate the ratio of projected linear sizes of radio galaxies to quasars. The number of total sources in a bin and the number of quasars in that bin are used to calculate the quasar fraction. The uncertainties were determined via standard error propagation methods, except for the case of the quasar fractions for the LOFAR sample, where we used small-number counting uncertainties following the prescription in Gehrels (1986). We assume that the error in spectroscopic redshift is negligible compared to the other measurement errors, and set this to zero.

We first examine the measured properties of radio galaxies and quasars by looking at how their linear sizes correlate with both power and redshift. This is shown in Fig. 2.5. There is no clear correlation between linear size and power.

Table 2.1: A summary of the different radio samples. The first line for each sample shows the parameters for the entire sample.

		Radio galaxies					Quasars		
	z range	No.	Mean z	Mean Linear Size [kpc]	D_A Correction	Corrected Linear Size [kpc]	No.	Mean z	Mean Linear Size [kpc]
LOFAR	≤ 3.25	44	1.16	228	1.02	233	16	1.84	76
	$0 < z \leq 1.5$	31	0.73	332	1.00	333	6	1.02	116
	$1.5 < z$	13	2.18	72	1.00	72	10	2.33	52
3CRR	≤ 2.01	111	0.49	300	1.25	375	59	0.82	196
	$0 < z \leq 0.5$	67	0.17	570	1.06	603	18	0.23	320
	$0.5 < z$	44	0.99	228	1.06	241	41	1.08	141
MRC	≤ 3.16	264	0.78	145	1.10	160	88	1.13	180
	$0 < z \leq 1$	199	0.43	223	1.02	227	48	0.66	242
	$1 < z$	65	1.73	86	1.02	88	40	1.69	105

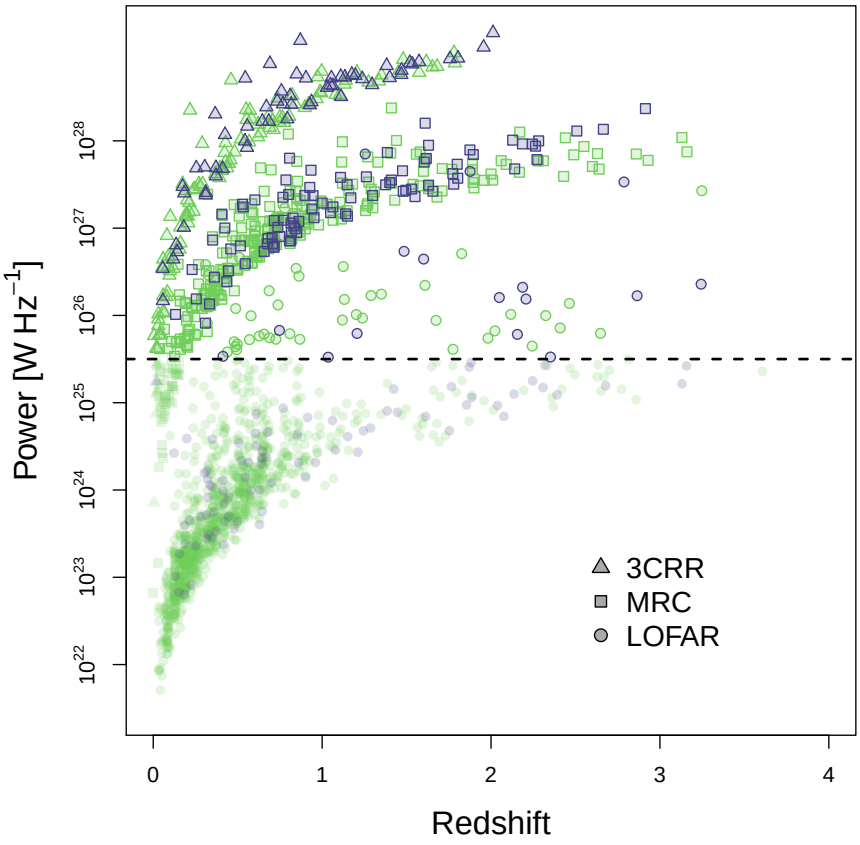

Figure 2.4: Power vs. redshift for the two samples described in this section plus the LOFAR sample. Only sources with spectroscopic redshifts are used, and above powers of $P_{150} > 10^{25.5}\,\mathrm{W\,Hz^{-1}}$ at 150 MHz. Spectral index information was used to convert measured power to P_{150} for the MRC and 3CRR samples. Green points represent radio galaxies and purple points represent quasars.

There does appear to be a correlation between linear size and redshift, with smaller objects found at higher redshifts. The anti-correlation of angular size with redshift is consistent with previous studies (Ker et al., 2012; Neeser et al., 1995; Wardle & Miley, 1974; Miley, 1968) which also find more compact radio sources at higher redshifts.

To quantify the dependence of size on redshift we use the same Partial-rank analysis as described in Section 2.3 of Neeser et al. (1995). Assuming a functional form of size $D \propto (1+z)^{-n}$ where n is the 'evolution strength,' we let n vary in steps of 0.001 over the range $0 \leq n \leq 3$. For each value of n we multiplied the source sizes by $(1+z)^n$ and calculated the Partial-rank statistic for D, z given P. The value of n that produced a statistic of 0 was taken as the evolution strength, and the upper and lower errors correspond to where the statistic was ± 1. We find evolution strengths of $n = 1.988^{+0.252}_{-0.270}$ for all radio galaxies and quasars considered together, $n = 2.051^{+0.391}_{-0.436}$ for radio galaxies, and $n = 1.773^{+0.288}_{-0.275}$ for quasars. These values all agree within the uncertainties, indicating that quasars and radio galaxies have the same evolution strength. The values are also in excellent agreement with Neeser et al. (1995), who find an evolution strength for galaxies and quasars of $n = 1.71^{+0.40}_{-0.48}$ for a flat universe.

We repeat the same exercise but looking at the Partial-rank statistic for D, P given z. Using the functional form $D \propto P^m$, we multiply the sources sizes by P^{-m} and vary m in steps of 5×10^{-5} from -1 to 1. The values of m that produce statistics of 0 are consistent with $m = 0$ for all samples. Specifically, for all sources we find $m = (1.5^{+3}_{-1.5}) \times 10^{-4}$, for radio galaxies we find $m = (2^{+2.5}_{-2}) \times 10^{-4}$, and for quasars we find $m = (5 \pm 5) \times 10^{-5}$. We therefore conclude that there is no intrinsic relationship between power and size.

We next investigate how the ratio between radio galaxy and quasar linear sizes evolves with power and with redshift, see Fig. 2.6. The 3CRR and LOFAR samples show size ratios larger than unity: the 3CRR sample has size ratios of 1.89 ± 0.41 (low z) and 1.71 ± 0.34 (high z) and the LOFAR sample has size ratios of 2.88 ± 0.97 (low z) and 1.38 ± 0.81 (high z). The MRC sample shows size ratios consistent with unity, with 0.93 ± 0.15 (low z) and 0.84 ± 0.21 (high z). There is no clear trend with either redshift or power. This indicates that the linear size ratio remains the same for a large range of powers and out to higher redshifts. The fact that the linear size ratio does not clearly evolve with either power or redshift implies that the populations of radio galaxies and quasars *always* have the same relative sizes.

Finally we investigate how the quasar fraction depends on the radio galaxy to quasar linear size length ratio. The results are shown in Fig. 2.7. There are

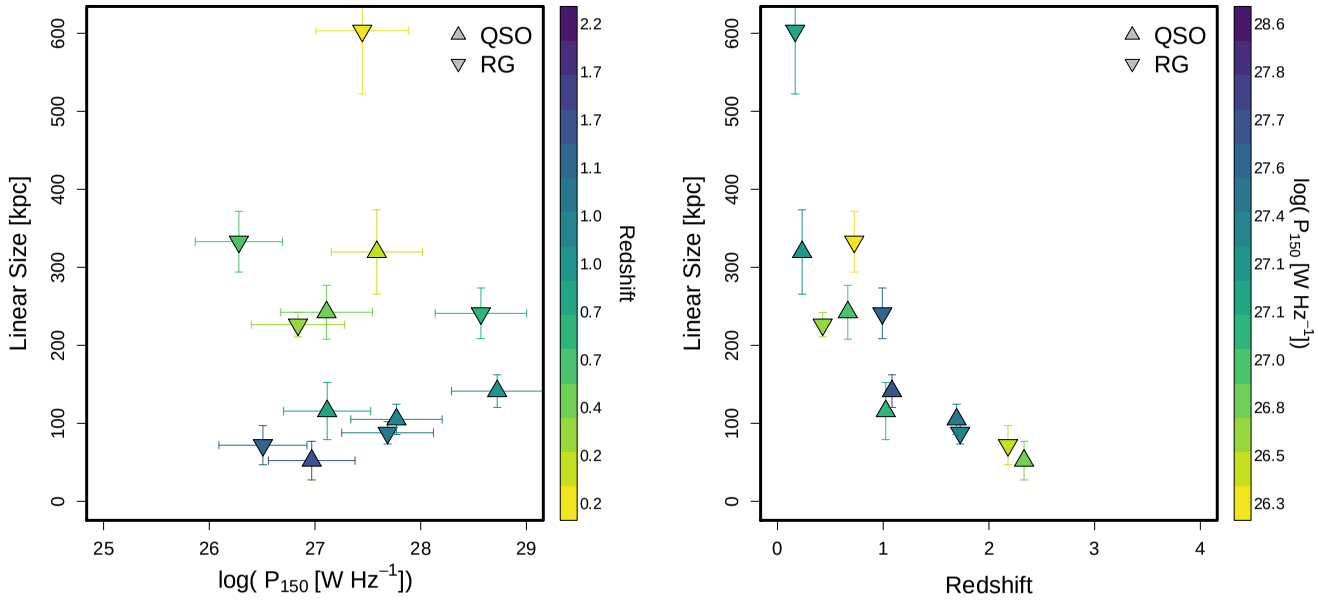

Figure 2.5: The linear sizes of quasars (triangles) and radio galaxies (inverted triangles) plotted against power ($left$) and ($redshift$). The points are coloured according to the colour bar to the right of each plot and show the redshift ($left$) and power ($right$).

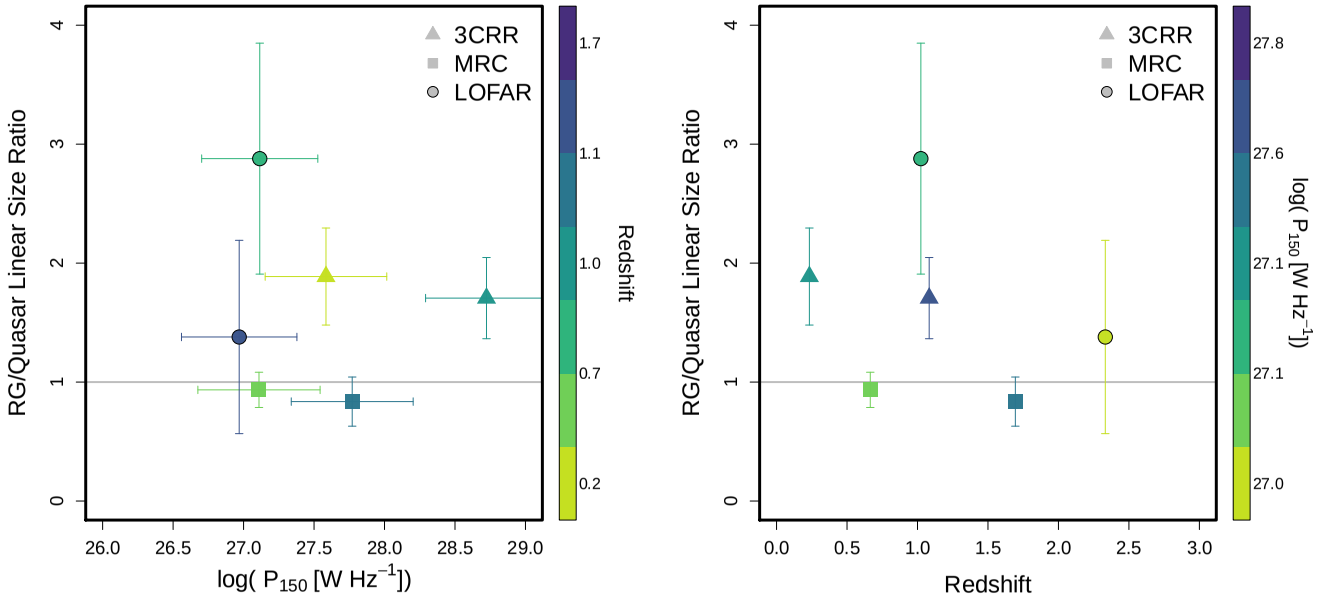

Figure 2.6: The radio galaxy to quasar linear size ratios plotted against power ($left$) and redshift ($right$). The symbol shapes represent the sample, with squares for the MRC, triangles for the 3CRR, and circles for the LOFAR samples. The colour axes are redshift ($left$) and power ($right$). The horizontal gray lines indicate where the linear size ratio is unity.

two groups of points in this plot, one group at quasar fractions of ~ 0.2 and one group at fractions of ~ 0.6 and above. The group of points with quasar fractions of ~ 0.2 corresponds to the lower redshift bins for all samples, while the second group of points corresponds to the higher redshift bins. For the low-redshift bins, the quasar fraction does not appear to evolve with the linear size ratio. For the high-redshift bins, the quasar fraction is correlated with the linear size ratio, and increases from 0.6 to almost unity.

2.5 Discussion

For the discussion, we first consider how the radio data can be interpreted given an orientation-based unification scenario. We then discuss the possibilities if evolution rather than orientation is the dominant effect that explains the data.

2.5.1 Orientation Interpretation

First we consider a scheme where the observed fraction of quasars depends *only* on viewing angle, which is supported by other observational evidence. For example, Antonucci & Ulvestad (1985) used high-resolution observations of blazars to show that they are consistent with being normal radio galaxies viewed along the jet axis. Observed differences in depolarisation of radio lobes (the Laing-Garrington effect) also indicate orientation effects, as the approaching (receding) jet will appear less (more) depolarised due to differential Faraday rotation in the ambient medium along the line of sight (Garrington et al., 1988). In some cases, this can cause sources close to the line of sight (i.e., quasars) to appear one-sided as the receding jet drops below the sensitivity limit. If we assume that all quasars in our LOFAR sample are one-sided and multiply their sizes by a factor of two to account for this, we still find a linear size ratio of radio galaxies to quasars of 1.53 ± 0.48. This is still above unity and therefore consistent with an orientation scheme. This is the *smallest* that the ratio could possibly be, as some quasars have clearly resolved double structure.

The radio orientation is clearly linked to the orientation of the torus/accretion disk, as shown by the detection of significant optical polarisation aligned with the radio jets in nearby galaxies (e.g., Schmidt & Smith, 2000; Antonucci, 1982). The observed properties of strong line AGN (HERGs) at wavelengths other than radio are consistent with orientation schemes, mostly due to the presence of a dusty obscuring structure. For example, the presence of broad lines in polarised light of Type 1 AGN (narrow line galaxies) is powerful evidence for hidden quasars whose light is reflected outside of the obscuring structure (e.g., Cohen et al., 1999; Ogle et al., 1997; Antonucci, 1984).

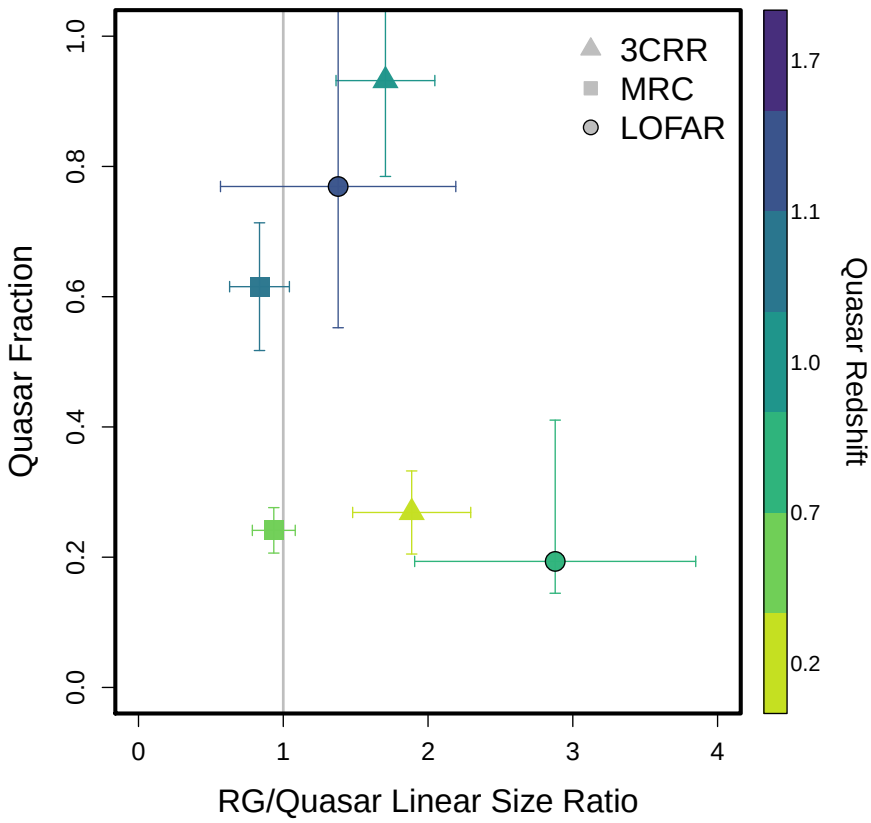

Figure 2.7: The quasar fraction vs. radio galaxy to quasar linear size ratio. Each sample is represented by symbols of different shapes as indicated in the legend. The gray line shows where the ratio between linear sizes of radio galaxies and quasars is unity. The color axis shows redshift.

The unification of observable characteristics of HERGs via orientation predicts several key observable characteristics with which we can compare our results. First, the projected linear sizes of quasars should on average be smaller than the projected linear sizes of radio galaxies. The new LOFAR data are consistent with this, as we found a linear size ratio of 3.1 ± 1.0 (for radio galaxies to quasars). For a population of randomly oriented sources, we can calculate the angle (between 0 and 90 degrees) which would define the division between the two populations. For the LOFAR sample this is $42.8^{+5.4}_{-6.0}$ degrees, which is in agreement with the value of 44.4 degrees found for the original 3CRR sample (Barthel, 1989). That would mean that quasars have their radio jets oriented between 0 degrees (line of sight) and 42.8 degrees, while radio galaxies have jets oriented between 42.8 degrees and 90 degrees (plane of sky).

Second, beamed radio sources with flat spectra should be oriented close to the line of sight, and therefore also be smaller on average than steep-spectrum sources. The LOFAR data is also consistent with this scenario, and the linear size ratio is 4.4 ± 1.4, even larger than the linear size ratio for radio galaxies/quasars. The angle of division between flat and steep spectrum sources is $35.2^{+5.2}_{-5.9}$ degrees. This is consistent with the idea that flat-spectrum sources are mostly beamed radio jets that are oriented close to the line of sight.

Finally, the quasar fraction should be directly correlated with the linear size ratio if *only* orientation is responsible for whether or not we observe a quasar. When dividing the samples into low and high redshift bins, we find that the quasar fraction remains constant with increasing linear size ratios for the low redshift bins, and increases for the high redshift bins. Since the 3CRR and MRC samples are virtually spectroscopically complete, and we have shown in Section 2.2 that we do not believe to be missing a substantial population of sources from the LOFAR sample, the correlation of quasar fraction with linear size at high redshift appears to be real, which is consistent with being due to orientation. Reducing the uncertainties on the LOFAR data point will help unambiguously determine if the low-redshift data is consistent with a constant or increasing quasar fraction.

Overall, we find that the results are consistent with an orientation-based unification scenario. The LOFAR and 3CRR samples show similar trends, while the MRC sample does not show systematically different sizes for quasars and radio galaxies.

2.5.2 Evolutionary Interpretation

Another possibility is that radio galaxies and quasars are linked through an evolutionary scheme rather than by orientation alone. In such a scheme, radio jets would be triggered when quasars become active. The radio jets would grow and finally when the quasar reaches an inactive state the source would be classified as a radio galaxy. The measured quasar fraction in this case would be interpreted as the fraction of time a source spends as an active quasar. In the LOFAR sample the sizes of radio galaxies are on average larger than the sizes of quasars, which is consistent with this evolutionary scheme. However, evolution alone cannot explain observational effects like the Laing-Garrington effect or the presence of scattered quasar light in radio galaxies (e.g., Jackson et al., 1998).

If an evolutionary scheme holds, the fact that higher quasar fractions are seen for the higher redshift bins would mean that either higher redshift sources spend a longer portion of their lives as quasars before becoming radio galaxies, or that there are simply far more young quasars than old radio galaxies at high redshift. If it is true that higher redshift sources spend longer portions of their lives as quasars, the radio jets would have to grow more slowly to be consistent with Fig. 2.6, where we see no change in the linear size ratio with redshift. Slower growth of radio jets could be due to the higher density ambient medium expected at high redshift, but it would not change the amount of time that a quasar is active. The data is therefore inconsistent with this scenario. If there are simply more young quasars at higher redshift, we would expect to see larger linear size ratios between quasars and radio galaxies at high redshift, which is again inconsistent with our results. This could possibly be rectified if *all* sources at high redshift were younger than those at low redshift, but a scenario where this would be the case is hard to imagine.

2.6 Conclusions

In this paper we used a new LOFAR survey of the Boötes field to show that the projected linear sizes of steep-spectrum radio sources are on average 4.4 ± 1.4 times larger than those of flat-spectrum radio sources. This is consistent with an orientation scheme for radio jets, where beamed flat-spectrum radio sources lie closer to the line of sight and therefore have smaller projected sizes.

We have also shown for radio galaxies and quasars in the LOFAR survey, as identified by AGES criteria, the projected linear sizes of radio galaxies are on average 3.1 ± 1.0 times larger than those of quasars. This is also consistent with an orientation scheme, where the presence of a dusty obscuring torus prevents the identification of a quasar unless the radio jets are preferentially aligned

closer to the line of sight.

When combining the new LOFAR measurements with two previous surveys and separating each sample into low and high redshift bins, we find no clear trend between the linear size ratio of radio galaxies to quasars and either power or redshift. This suggests that the populations of radio galaxies and quasars *always* have the same relative sizes. For the low redshift bins, we find that the quasar fraction remains ~ 0.2 even as the linear size ratio changes, although the uncertainties are still large. The MRC sample also consistently measures a linear size ratio of unity, and more data is necessary to resolve the inconsistency of the 3CRR/LOFAR measured size ratios and the MRC measured size ratio.

We conclude that the data presented here are consistent with an orientation-based unification scheme. We have found that on average the projected sizes of radio galaxies are larger than quasars for both the LOFAR and 3CRR samples, and that this does not depend on power or redshift.

Ultimately the LOFAR Tier 1 survey will cover the Northern sky above declination 0 degrees, providing millions of radio sources. Spectroscopic redshifts and host galaxy identifications will be provided by a survey with the William Herschel Telescope Enhanced Area Velocity Explorer (WEAVE) which goes online March 2018. The WEAVE-LOFAR survey (Smith et al., in preparation, Smith, 2015) is dedicated to providing this information for $\sim 10^6$ LOFAR-detected sources in the Tier 1 survey. Ultimately with this information we will be able to break the degeneracy between orientation and evolutionary effects in unification schemes.

Acknowledgements

LKM acknowledges financial support from NWO Top LOFAR project, project n. 614.001.006.

Bibliography

Antonucci R. R. J., 1982, Nature, 299, 605

Antonucci R. R. J., 1984, ApJ, 278, 499

Antonucci R., 1993, ARA&A, 31, 473

Antonucci R. R. J., Ulvestad J. S., 1985, ApJ, 294, 158

Baker J. C., Hunstead R. W., Kapahi V. K., Subrahmanya C. R., 1999, ApJS, 122, 29

Barthel P. D., 1989, ApJ, 336, 606

Barthel P. D., Hooimeyer J. R., Schilizzi R. T., Miley G. K., Preuss E., 1989, ApJ, 336, 601

Best P. N., Heckman T. M., 2012, MNRAS, 421, 1569

Best P. N., Röttgering H. J. A., Lehnert M. D., 1999, MNRAS, 310, 223

Best P. N., Kauffmann G., Heckman T. M., Brinchmann J., Charlot S., Ivezić Ž., White S. D. M., 2005, MNRAS, 362, 25

Brown M. J. I., Dey A., Jannuzi B. T., Brand K., Benson A. J., Brodwin M., Croton D. J., Eisenhardt P. R., 2007, ApJ, 654, 858

Brown M. J. I., et al., 2008, ApJ, 682, 937

Cohen M. H., Ogle P. M., Tran H. D., Goodrich R. W., Miller J. S., 1999, AJ, 118, 1963

Evans D. A., Worrall D. M., Hardcastle M. J., Kraft R. P., Birkinshaw M., 2006, ApJ, 642, 96

Fanaroff B. L., Riley J. M., 1974, MNRAS, 167, 31P

Garrington S. T., Leahy J. P., Conway R. G., Laing R. A., 1988, Nature, 331, 147

Gehrels N., 1986, ApJ, 303, 336

Grimes J. A., Rawlings S., Willott C. J., 2004, MNRAS, 349, 503

Hardcastle M. J., Evans D. A., Croston J. H., 2006, MNRAS, 370, 1893

Ho L. C., 2008, ARA&A, 46, 475

Jackson N., Tadhunter C., Sparks W. B., 1998, MNRAS, 301, 131

Jannuzi B. T., Dey A., 1999, in Bunker A. J., van Breugel W. J. M., eds, Astronomical Society of the Pacific Conference Series Vol. 193, The Hy-Redshift Universe: Galaxy Formation and Evolution at High Redshift. p. 258

Kapahi V. K., Athreya R. M., van Breugel W., McCarthy P. J., Subrahmanya C. R., 1998a, ApJS, 118, 275

Kapahi V. K., Athreya R. M., Subrahmanya C. R., Baker J. C., Hunstead R. W., McCarthy P. J., van Breugel W., 1998b, ApJS, 118, 327

Ker L. M., Best P. N., Rigby E. E., Röttgering H. J. A., Gendre M. A., 2012, MNRAS, 420, 2644

Kochanek C. S., et al., 2012, ApJS, 200, 8

Laing R. A., Riley J. M., Longair M. S., 1983, MNRAS, 204, 151

Larson R. B., 2010, Nature Physics, 6, 96

Miley G. K., 1968, Nature, 218, 933

Narayan R., Yi I., 1994, ApJL, 428, L13

Neeser M. J., Eales S. A., Law-Green J. D., Leahy J. P., Rawlings S., 1995, ApJ, 451, 76

Ogle P. M., Cohen M. H., Miller J. S., Tran H. D., Fosbury R. A. E., Goodrich R. W., 1997, ApJL, 482, L37

Ogle P., Whysong D., Antonucci R., 2006, ApJ, 647, 161

Planck Collaboration et al., 2015, preprint, (arXiv:1502.01589)

Quataert E., 2001, in Peterson B. M., Pogge R. W., Polidan R. S., eds, Astronomical Society of the Pacific Conference Series Vol. 224, Probing the Physics of Active Galactic Nuclei. p. 71

Rigby E. E., Best P. N., Brookes M. H., Peacock J. A., Dunlop J. S., Röttgering H. J. A., Wall J. V., Ker L., 2011, MNRAS, 416, 1900

Schmidt G. D., Smith P. S., 2000, ApJ, 545, 117

Shakura N. I., Sunyaev R. A., 1973, A&A, 24, 337

Singal A. K., 2014, AJ, 148, 16

Singal A. K., Singh R. L., 2013, MNRAS, 435, L38

Smith D. J. B., 2015, preprint, (arXiv:1506.05630)

Stern D., et al., 2005, ApJ, 631, 163

Tasse C., Best P. N., Röttgering H., Le Borgne D., 2008, A&A, 490, 893

Taylor M. B., 2005, in Shopbell P., Britton M., Ebert R., eds, Astronomical Society of the Pacific Conference Series Vol. 347, Astronomical Data Analysis Software and Systems XIV. p. 29

Urry C. M., Padovani P., 1995, PASP, 107, 803

Wardle J. F. C., Miley G. K., 1974, A&A, 30, 305

Whysong D., Antonucci R., 2004, ApJ, 602, 116

Williams W. L., 2015, PhD thesis, Leiden University
Williams W. L., et al., 2016, preprint, (arXiv:1605.01531)
Willott C. J., Rawlings S., Blundell K. M., Lacy M., 1999, MNRAS, 309, 1017
de Vries W. H., Morganti R., Röttgering H. J. A., Vermeulen R., van Breugel W., Rengelink R., Jarvis M. J., 2002, AJ, 123, 1784
van Haarlem M. P., et al., 2013, A&A, 556, A2